environmental and earth sciences proceedings

MDPI

Proceeding Paper

Mechanistic Insights into Phenol Adsorption and Mass Transport on Multi-Walled Carbon Nanotubes: A Phenomenological Modeling Approach with Sensitivity Analysis †

Thiago Ferro de Oliveira [1,2,3,*] and Simoni Margareti Plentz Meneghetti [2,3]

[1] Institute of Mathematics, Federal University of Alagoas, Maceió 57072-970, Brazil
[2] Postgraduate Program in Chemical Engineering, Federal University of Alagoas, Maceió 57072-970, Brazil; simoni.plentz@iqb.ufal.br
[3] Catalysis and Chemical Reactivity Group (GCAR), Chemistry Department, Federal University of Alagoas, Maceió 57072-970, Brazil
* Correspondence: thiago.oliveira@im.ufal.br
† Presented at the 1st International Online Conference on Environment (IOCE 2026), 2–4 March 2026; Available online: https://sciforum.net/event/IOCE2026.

Abstract

The removal of phenol from contaminated effluents presents an industrial challenge owing to its toxicity at trace concentrations. Multi-walled carbon nanotubes (MWCNTs) have been studied as adsorbents for this purpose, given their high adsorption capacity and ease of separation. This work presents a theoretical phenomenological and numerical analysis of mass transport coupled to phenol adsorption on MWCNTs (external diameter $d_{ext} = 50$ nm), parameterized using published experimental equilibrium data acquired under neutral pH conditions at 298 K. The mathematical model incorporates an effective pore diffusivity ($D_e = 3.213 \times 10^{-10}$ m^2/s) derived from pore structure parameters and describes three distinct scenarios: (1) pure physical adsorption via a modified Fick's Second Law; (2) coupled diffusion–reaction with 0.5-order kinetics, herein treated as an empirical kinetic ansatz with phenomenological divergence from lumped empirical models (PFO/PSO); and (3) a parametric and sensitivity analysis on particle size (1–100 nm) and inlet concentration (1–5 mg/L). Numerical solutions confirm a Thiele modulus $\phi \ll 1$ across the tested range, indicating a kinetically controlled regime with effectiveness factor $\eta \approx 1.0$, and validate the theoretical scaling $\phi \propto C_s^{-0.25}$. During effluent polishing operations (reduction from 5 to 1 mg/L), the relative diffusive resistance increases by 49.5%, suggesting proportional increases in contact time or adsorbent dosage are required. A one-at-a-time (OAT) sensitivity analysis on D_e, κ, and k_{obs} confirms that the kinetically controlled regime is preserved across plausible parameter ranges. The nanoscale architecture of MWCNTs reduces theoretical intraparticle diffusional resistance by several orders of magnitude relative to macroscopic granular adsorbents. We emphasize that these conclusions describe theoretical mass-transport advantages; experimental and pilot-scale validation under realistic, multi-component wastewater conditions remains an essential step before industrial deployment.

Keywords: aromatic pollutants; graphitic networks; predictive simulation; solid–liquid interface; environmental decontamination; Langmuir isotherm; π–π stacking; hydrogen bonding; hydrophobic interactions; surface heterogeneity

Check for updates

Academic Editor: Gabriella Fiorentino

Published: 4 August 2026

Copyright: © 2026 by the authors. Licensee MDPI, Basel, Switzerland. This article is an open access article distributed under the terms and conditions of the Creative Commons Attribution (CC BY) license.

1. Introduction

The remediation of phenol-contaminated effluents constitutes a challenge in the environmental and chemical industries [1,2]. Phenol, even at trace concentrations, exhibits acute toxicity to aquatic organisms and represents an environmental hazard [3,4]. Industries such as petroleum refining, resin manufacturing, pharmaceuticals, and biomedical waste generation routinely discharge phenolic-rich effluents, and a wide variety of treatment strategies, ranging from biological degradation and advanced oxidation to adsorption, have been investigated [4–6].

Multi-walled carbon nanotubes (MWCNTs) have been investigated as adsorbents for organic pollutants, given their large specific surface area, structural properties, and high adsorption capacity [7,8]. At the molecular level, phenol adsorption on nanocarbon surfaces is governed by a combination of mechanisms, including dispersion forces, π–π stacking, hydrophobic interactions, and hydrogen bonding, the relative contribution of which depends on the pH of the medium and the surface chemistry [8,9]. Studies have further shown that surface functionalization (e.g., oxidation, sulfonation, or plasma activation) can modify the adsorption capacity, kinetics, and selectivity of MWCNTs toward phenolic and aromatic pollutants [6,8,9].

Nano-adsorbents have demonstrated improvements over conventional granular activated carbons in terms of accessible surface area and external mass-transfer characteristics [5,6]. Nevertheless, there is a recognized gap between (i) molecular- or batch-scale equilibrium studies and (ii) reactor-scale process design, particularly because diffusion–reaction coupling, surface heterogeneity, and competitive adsorption are rarely combined into a single, transparent mathematical framework. To address this gap in a deliberately limited and theoretical way, the present work develops a phenomenological and numerical analysis of intraparticle mass transport coupled with phenol adsorption on MWCNTs. This article is an extended and revised version of our preliminary study presented at the 1st International Online Conference on Environments [10]. Relative to that conference contribution, it incorporates a corrected mass-transport parameterization, namely the intraparticle porosity computed from the specific pore volume and the resulting effective and apparent diffusivities, together with a one-at-a-time sensitivity analysis, an explicit comparison with pseudo-first- and pseudo-second-order kinetics, and a critical discussion of the model assumptions. These additions modify some of the intermediate numerical values reported at the conference while preserving the qualitative conclusions.

The study is parameterized and benchmarked against published experimental equilibrium data, specifically acquired under neutral pH conditions at 298 K [7,11]. The methodology evaluates three modeling scenarios, ranging from pure physical diffusion to parametric kinetic regimes, in order to elucidate the mass-transport limitations inherent to nanoscale carbonaceous adsorbents. We position this contribution as a theoretical exploration providing mechanistic insight, and we discuss its limitations and the conditions under which its conclusions can be expected to remain valid in real wastewater systems.

2. Characterization and Theoretical Foundation

2.1. Physicochemical Properties and Operating Conditions

MWCNTs consist of concentric graphite cylinders with a hexagonal structure. Based on the experimental data parameterized in this study [7], the structural properties are defined as follows (symbols are also summarized in the Abbreviations list at the end of the manuscript):

https://doi.org/10.3390/eesp2026042022

$$\begin{aligned} d_{ext} &= 50\ \text{nm} \quad \text{(particle external diameter)};\\ d_{int} &= 5\text{–}10\ \text{nm} \quad \text{(internal pore diameter)};\\ \rho_{true} &= 2100\ \text{kg/m}^3 \quad \text{(true graphitic density)};\\ \rho_s &= 100\ \text{kg/m}^3 \quad \text{(bulk density of the packed adsorbent)};\\ V_p &= 0.8 \times 10^{-3}\ \text{m}^3/\text{kg} \quad \text{(specific pore volume)};\\ \varepsilon_p &= 0.627 \quad \text{(intraparticle porosity, dimensionless)};\\ \text{SSA} &= 300\ \text{m}^2/\text{g} \quad \text{(specific surface area, BET)}. \end{aligned} \tag{1}$$

The intraparticle porosity is computed from the specific pore volume and the skeletal density as $\varepsilon_p = V_p/(V_p + 1/\rho_{true}) = 0.627$, which corresponds to the fraction of the particle volume occupied by pores and yields an apparent particle density $\rho_{ap} = \rho_{true}\,(1 - \varepsilon_p) = 784\ \text{kg/m}^3$. The values adopted for d_{ext} and for the specific surface area are the midpoints of the ranges reported in [7] (40–60 nm and 40–600 m^2/g).

A tortuosity factor of $\kappa = 2.0$ (dimensionless) is adopted for the pore network. In the absence of a direct structural measurement, this value is taken as representative: it lies within the range commonly used for packed beds of particles and consolidated porous media, where the tortuosity factor relates the effective diffusivity to the molecular diffusivity through the available pore-volume fraction [12,13]. The sensitivity of the results to this choice is examined in Section 6.3. Phenol is an aromatic compound with $\text{p}K_a \approx 10$. Under the standard operating conditions established for this numerical analysis (neutral pH and 298 K), phenol exists predominantly in its non-ionic molecular form, favouring hydrophobic interactions and hydrogen bonding with the uncharged carbon surface. The molecular diffusivity in pure water at 298 K is $D_{AB} = 1.025 \times 10^{-9}\ \text{m}^2/\text{s}$ [11].

2.2. Effective Diffusivity

In porous media, the diffusive flux is restricted by the pore geometry and the available pore-volume fraction. Following the phenomenological analyses by Epstein [12] and van Brakel and Heertjes [13], which establish that the diffusive restriction scales with the tortuosity factor ($\kappa = \tau^2$) rather than linear tortuosity, the effective diffusivity (D_e) is defined as:

$$D_e = D_{AB}\,\frac{\varepsilon_p}{\kappa} \tag{2}$$

Applying the structural parameters from Equation (1) and adopting a representative tortuosity factor $\kappa = 2.0$:

$$D_e = 3.213 \times 10^{-10}\ \text{m}^2/\text{s} \tag{3}$$

In nano-adsorbents ($d_{ext} = 50$ nm), the intraparticle diffusion length is reduced by several orders of magnitude relative to macroscopic granular activated carbons.

3. Mathematical Development

The differential equation governing transport coupled with reaction/adsorption in porous media for spherical geometry with radial symmetry, derived from the mass balance over a differential volume element of the porous particle, is:

$$\varepsilon_p \frac{\partial C}{\partial t} + \rho_{ap} \frac{\partial q}{\partial t} = D_e \left[\frac{\partial^2 C}{\partial r^2} + \frac{2}{r} \frac{\partial C}{\partial r} \right] + R_A \tag{4}$$

where C is the local pore-fluid concentration of phenol [mol/m^3], q is the adsorbed-phase concentration [mol/kg], R_A is the reaction rate per unit apparent particle volume [$\text{mol/(m}^3\,\text{s)}$], D_e is the effective diffusivity [m^2/s], r is the radial coordinate [m], t is time [s], and R_p denotes the particle radius [m]. Boundary conditions impose symmetry at the centre,

$\partial C/\partial r|_{r=0} = 0$, and a prescribed surface concentration, $C(R_p, t) = C_s$. The corresponding initial condition is $C(r, 0) = 0$.

The methodological workflow integrating the experimental data, the mathematical model, and the three evaluated scenarios is illustrated in Figure 1.

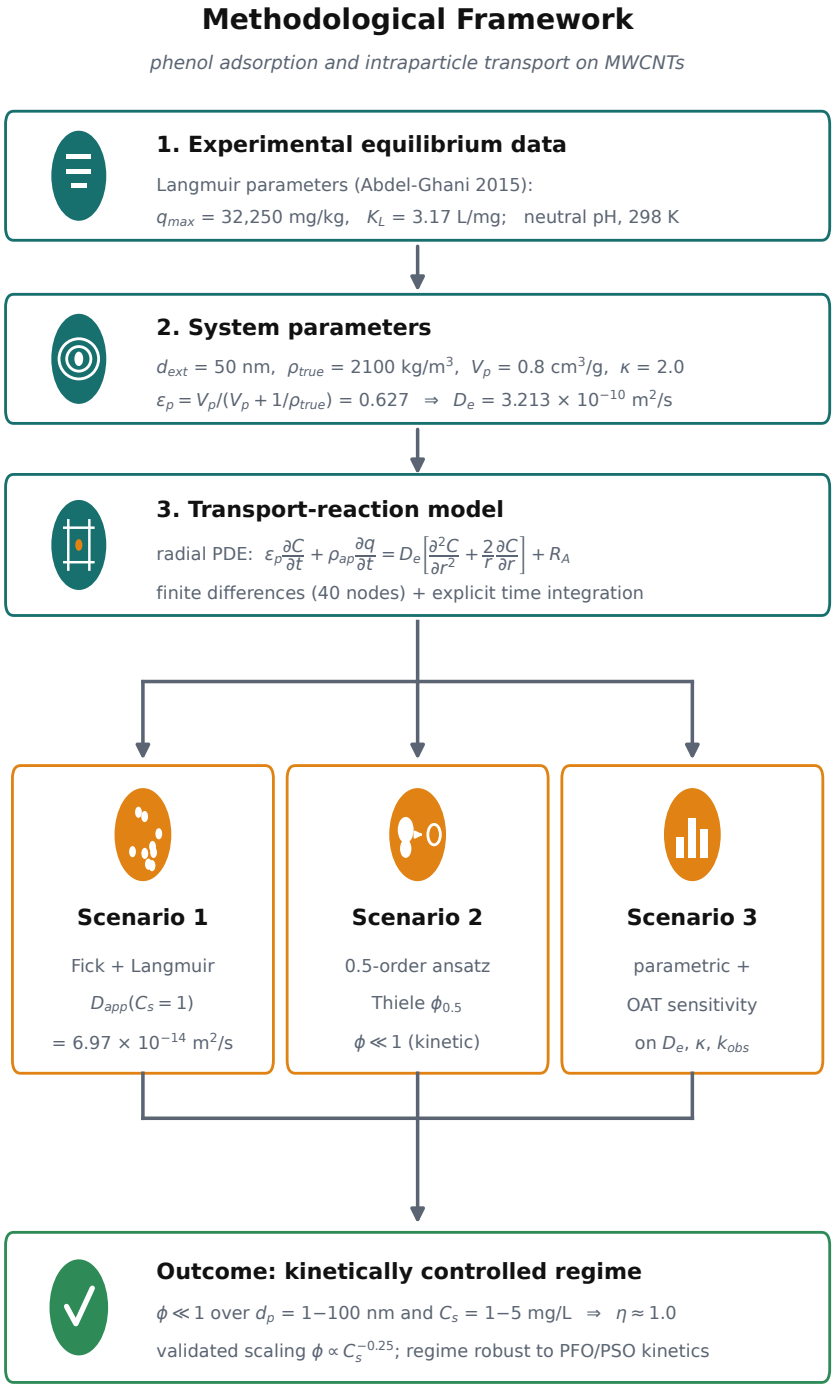

Figure 1. Methodological flowchart detailing the system of this work. The Langmuir equilibrium parameters shown in step 1 are those reported by Abdel-Ghani et al. [7].

4. Model Scenario 1: Pure Physical Adsorption

4.1. Analytical Formulation and Discussion of the Langmuir Assumption

In pure physical adsorption without chemical reaction, $R_A = 0$. The relationship between the pore-fluid and the adsorbed phase is described, in this scenario, by the Langmuir isotherm,

$$q = \frac{q_{max}\, K_L\, C}{1 + K_L\, C}, \tag{5}$$

parameterized with q_{max} = 32,250 mg/kg and K_L = 3.17 L/mg [7]. The Langmuir model assumes (i) a homogeneous surface, (ii) monolayer coverage, and (iii) energetically equivalent, non-interacting adsorption sites.

Limitations of the Langmuir Assumption for MWCNTs

Carbon nanotube surfaces are inherently heterogeneous, exhibiting graphitic basal planes, defect sites, and oxygen-bearing functional groups whose populations depend on the synthesis route and any post-treatment, such as acid oxidation, plasma functionalization, or sulfonation [8,9]. The adsorption of phenol onto these nanocarbon surfaces is driven by a combination of donor-acceptor π–π interactions (between the aromatic ring of phenol and the graphitic surface or electron-donor groups), hydrophobic effects, and hydrogen-bonding with oxygenated surface functionalities [7,14]. Consequently, multi-site behaviour, multilayer adsorption, and non-ideal energetics might conceptually be expected, especially at higher loadings.

Despite this inherent surface heterogeneity, primary experimental investigations report that the Langmuir isotherm provides a superior fit over the Freundlich model for the adsorption of phenol on MWCNTs and related carbonaceous adsorbents, indicating homogeneous monolayer coverage [7,14]. Therefore, the qualitative conclusions on the regime of operation (kinetic vs. diffusion-limited) are not expected to deviate in the dilute concentration range explored here.

Defining an apparent diffusivity

$$D_{app}(C) = \frac{D_e}{\varepsilon_p + \rho_{ap}\, \dfrac{dq}{dC}}, \tag{6}$$

the transport equation reduces to a modified Fick's Second Law:

$$\frac{\partial C}{\partial t} = D_{app}(C)\left[\frac{\partial^2 C}{\partial r^2} + \frac{2}{r}\,\frac{\partial C}{\partial r}\right] \tag{7}$$

4.2. Numerical Solution: Concentration-Dependent Apparent Diffusivity

Spatial discretization via central finite differences (40 radial nodes) and explicit temporal integration yield concentration-dependent apparent diffusivities. For C_s = 1.0 mg/L, $D_{app} \approx 6.973 \times 10^{-14}$ m^2/s, leading to a characteristic intraparticle time $\tau_c = R_p^2/D_{app} \approx 8.963 \times 10^{-3}$ s. For C_s = 5.0 mg/L, $D_{app} \approx 1.136 \times 10^{-12}$ m^2/s, with $\tau_c \approx 5.501 \times 10^{-4}$ s. The reduction in D_{app} relative to D_e reflects the coupling between intraparticle diffusion and rapid adsorption-site filling, associated with the high $\rho_{ap}(dq/dC)$ retardation factor.

5. Model Scenario 2: Half-Order Reaction Kinetics

5.1. Justification of the 0.5-Order Kinetic Ansatz and Comparison with Classical Models

5.1.1. Physical Motivation

A half-order rate law ($R_A = -k_{obs}\, C^{0.5}$) does not correspond to a single elementary step. It is adopted here as an empirical kinetic ansatz, motivated by the observation that apparent fractional orders can emerge in systems with a distribution of site energies and with coupling between site saturation and intraparticle diffusion. The 0.5-order form is retained for two instrumental reasons: (i) it admits a closed-form Thiele modulus, and (ii) it provides a representative bound on ϕ relative to first-order kinetics. No claim is made that this reaction order is mechanistically established for phenol–MWCNT systems; its adequacy is assessed by comparison with the PFO and PSO models below.

5.1.2. Comparison with PFO and PSO Models

The pseudo-first-order (PFO) and pseudo-second-order (PSO) models are the most widely used phenomenological descriptions of adsorption kinetics in batch experiments, having been extensively applied to evaluate the uptake of phenolic compounds and dyes on diverse macroscopic and nanostructured adsorbents [4,6,8,9]. Specifically for the phenol–MWCNT system, experimental investigations have reported that the PSO model provides a superior fit to the kinetic data over the PFO model [7]. The dominance of the PSO kinetic behavior has also been corroborated for the adsorption of cationic dyes onto functionalized and oxidized MWCNTs [8,9].

5.2. Analytical Formulation

For a half-order reaction with rate constant k_{obs} in units of $\mathrm{mol}^{0.5}\,\mathrm{m}^{-1.5}\,\mathrm{s}^{-1}$, the dimensionless steady-state mass balance yields the Thiele modulus

$$\phi_{0.5}^2 = \frac{k_{obs}\, R_p^2}{D_e \sqrt{C_s}} \tag{8}$$

A value $k_{obs} = 10^{-6}$ $\mathrm{mol}^{0.5}\,\mathrm{m}^{-1.5}\,\mathrm{s}^{-1}$ was adopted as a representative estimate for this order-of-magnitude analysis. The sensitivity of the results to this value is examined in Section 6.3.

For $C_s = 1.0$ mg/L, $\phi_{0.5} = 4.34 \times 10^{-6}$. For $C_s = 5.0$ mg/L, $\phi_{0.5} = 2.91 \times 10^{-6}$. Since $\phi \ll 1$ in both cases, the effectiveness factor (η) approaches 1.0, indicating the absence of internal diffusion limitations.

5.3. Numerical Solution: Internal Concentration Profiles

The boundary value problem was solved numerically using a 4th-order explicit Runge–Kutta method. The resulting internal concentration profiles $u(\xi)$ are essentially flat across the particle radius, with $u(0) \approx u(1) = 1.0$, corroborating the theoretical $\eta \approx 1.0$ and the dominance of the kinetically controlled regime.

6. Model Scenario 3: Parametric and Sensitivity Analyses

6.1. Particle Size Sensitivity (1–100 nm)

The Thiele modulus scales linearly with the particle radius ($\phi_{0.5} \propto R_p$), which appears as a unit-slope power law on the logarithmic axes of Figure 2A. Table 1 and Figure 2A present the parametric variation in particle size.

Table 1. Thiele modulus and effectiveness factor as a function of particle size at two representative inlet concentrations.

d_p (nm)	$\phi_{0.5}^{C_s=1.0\ \mathrm{mg/L}}$	$\phi_{0.5}^{C_s=5.0\ \mathrm{mg/L}}$	η	Regime
1	8.69×10^{-8}	5.81×10^{-8}	≈1.0000	Kinetic
5	4.34×10^{-7}	2.91×10^{-7}	≈1.0000	Kinetic
10	8.69×10^{-7}	5.81×10^{-7}	≈1.0000	Kinetic
20	1.74×10^{-6}	1.16×10^{-6}	≈1.0000	Kinetic
50	4.34×10^{-6}	2.91×10^{-6}	≈1.0000	Kinetic
100	8.69×10^{-6}	5.81×10^{-6}	≈1.0000	Kinetic

Even at the upper bound of the nanoscale (100 nm), ϕ remains below the threshold for diffusion limitation, indicating a kinetically controlled regime with complete particle utilization ($\eta \approx 1.0$).

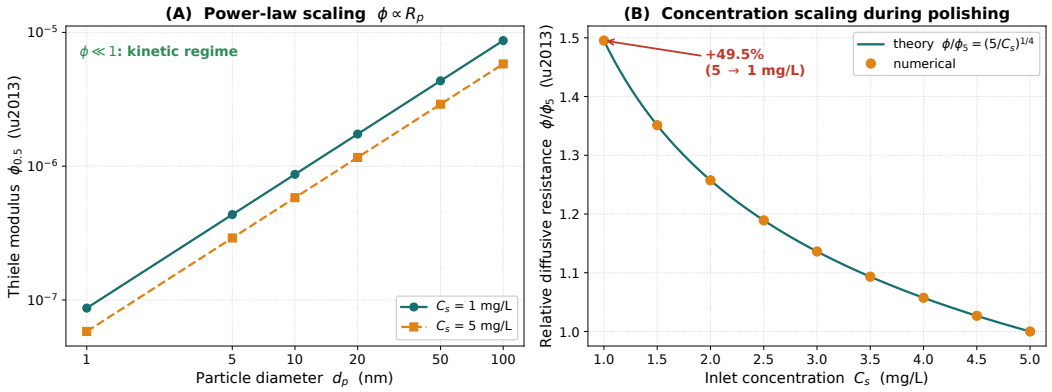

Figure 2. Parametric and sensitivity analyses of the half-order Thiele modulus. (**A**) Power-law scaling with particle size at $C_s = 1$ and 5 mg/L, the whole 1–100 nm range remaining kinetically controlled ($\phi \ll 1$). (**B**) Relative diffusive resistance ϕ/ϕ_5 versus inlet concentration, numerical solution against the theoretical scaling $(5/C_s)^{1/4}$.

6.2. Concentration Sensitivity (1–5 mg/L)

According to Equation (8), the Thiele modulus depends inversely on $\sqrt[4]{C_s}$, yielding the theoretical scaling $\phi \propto C_s^{-0.25}$.

The numerical integration matches the theoretical prediction (Table 2 and Figure 2B). The 49.5% increase in relative diffusive resistance during effluent polishing (reduction from 5.0 to 1.0 mg/L) suggests that achieving trace-level compliance requires proportionally greater contact times or higher adsorbent dosages.

Table 2. Dependence of the Thiele modulus on inlet concentration (evaluated at $d_p = 100$ nm): theoretical–numerical validation.

C_s (mg/L)	$\phi_{0.5}$	Ratio ϕ/ϕ_5 (Numerical)	ϕ/ϕ_5 (Theoretical)
1.00	8.69×10^{-6}	1.4953	1.4953
1.50	7.85×10^{-6}	1.3512	1.3512
2.00	7.31×10^{-6}	1.2574	1.2574
2.50	6.91×10^{-6}	1.1892	1.1892
3.00	6.60×10^{-6}	1.1362	1.1362
3.50	6.35×10^{-6}	1.0933	1.0933
4.00	6.14×10^{-6}	1.0574	1.0574
4.50	5.97×10^{-6}	1.0267	1.0267
5.00	5.81×10^{-6}	1.0000	1.0000

6.3. One-at-a-Time (OAT) Sensitivity and Uncertainty Considerations

To address the propagation of uncertainty arising from the chosen parameter values, a one-at-a-time (OAT) sensitivity analysis was carried out on three key inputs: the effective diffusivity D_e, the tortuosity factor κ used to compute it, and the apparent kinetic constant k_{obs}. Each parameter was varied by $\pm 50\%$ around its baseline value, and the resulting Thiele modulus was recomputed at $C_s = 1.0$ mg/L and $d_p = 50$ nm. The results are summarized in Table 3.

Even when the kinetic constant is increased by a factor of ten over its baseline value, the Thiele modulus remains below unity, indicating that the kinetically controlled conclusion is preserved against parameter uncertainty within the tested range. We note, however, that this OAT analysis explores parameter sensitivity in isolation and does not capture covariance effects; a future, fully Monte Carlo-based propagation, constrained by independent experimental measurements, would provide a more rigorous quantification.

Table 3. One-at-a-time sensitivity of the Thiele modulus to baseline parameter perturbations, evaluated at $C_s = 1.0$ mg/L and $d_p = 50$ nm. The kinetic regime is preserved across the entire tested range.

Parameter	Baseline	Range Tested	$\phi_{0.5}$ Range	Regime
D_e (m^2/s)	3.213×10^{-10}	±50%	3.55×10^{-6}–6.14×10^{-6}	Kinetic
κ (–)	2.0	1.0–3.0	3.07×10^{-6}–5.32×10^{-6}	Kinetic
k_{obs} ($mol^{0.5}\,m^{-1.5}\,s^{-1}$)	10^{-6}	10^{-7}–10^{-5}	1.37×10^{-6}–1.37×10^{-5}	Kinetic

Comparison with PFO/PSO Models

While the PFO and PSO models are widely employed to fit macroscopic batch adsorption data for phenol–MWCNT systems [7], they represent empirical approaches that aggregate external film transfer, intraparticle diffusion, and active-site binding into a single apparent rate. Substituting a macroscopic batch parameter (such as the PSO k_2) directly as an intrinsic volumetric sink term (R_A) in Fick's Second Law is phenomenologically invalid, as it leads to the double-counting of diffusional resistances. Therefore, an intrinsic Thiele modulus cannot be derived from PSO/PFO constants. Nevertheless, the kinetic dominance established by the present 0.5-order kinetics demonstrates that, at the nanoscale, the internal diffusion length is sufficiently short that mass transport does not restrict the overall adsorption rate.

6.4. Comparison with the Literature Values for D_e

The effective diffusivity calculated here ($D_e = 3.213 \times 10^{-10}$ m^2/s) is of the same order of magnitude as the intraparticle diffusivity of phenol measured in macroreticular adsorbents (7.7×10^{-10} m^2/s for phenol in Duolite ES861) [15], and lies within the range generally reported for small aromatic molecules in porous adsorbents (10^{-11}–10^{-9} m^2/s). This agreement provides a partial cross-check of the chosen structural parameters.

7. Discussion: Applicability and Limitations Under Real Wastewater Conditions

The phenomenological framework developed here was deliberately constructed under controlled, idealized conditions: neutral pH, isothermal operation at 298 K, and a single-solute system. Real industrial effluents differ in several important ways, and these differences must be made explicit before any conclusion is transferred to process design.

7.1. pH Effects

The protonation state of phenol ($pK_a \approx 10$) and the ionization of surface oxygen functionalities both depend on pH. As shown for related systems, decreasing pH below the point of zero charge of the adsorbent suppresses electrostatic contributions and can change the dominant interaction mode [8,9]. The current model is therefore expected to remain quantitatively meaningful only near the parameterization conditions.

7.2. Temperature Effects

Adsorption equilibrium constants and effective diffusivities both have non-trivial temperature dependences. The endothermic character of phenolic adsorption, evidenced for analogous systems [6], implies that the Langmuir constants and D_{AB} used here would shift at the higher operating temperatures sometimes encountered in industrial effluents.

7.3. Competitive Adsorption and Ionic Strength

Industrial effluents typically contain mixtures of organic pollutants, dyes, surfactants, and inorganic salts. Competitive adsorption can reduce phenol uptake [7], while ionic

strength modulates the strength of electrostatic and hydrogen-bonding interactions [8]. The current single-solute formulation does not account for these effects.

7.4. Applicability to Other Nano-Adsorbents

The quantitative framework employed here is not specific to MWCNTs. It rests on an intraparticle diffusion–reaction balance summarized by the Thiele modulus and the effectiveness factor, and it applies to any adsorbent for which (i) the particle geometry can be approximated by radial symmetry (spherical or cylindrical), (ii) the characteristic intraparticle diffusion length is of nanometric scale, and (iii) the equilibrium isotherm and an effective diffusivity are available. Under these conditions, the same analysis is transferable to other nanostructured carbonaceous and related adsorbents, such as graphene oxide and magnetic graphene oxide [16], single-walled carbon nanotubes, and functionalized nanoporous resins [6]. Conversely, the conclusion of negligible intraparticle diffusional resistance does not extend to adsorbents with macroscopic diffusion lengths, such as granular activated carbon or millimetre-sized pellets, for which intraparticle diffusion can become rate-controlling [15].

7.5. Reactor-Scale and Economic Considerations

The conclusions derived here describe intra-particle mass transport. External mass transfer, hydrodynamics, packing density, fouling, regeneration efficiency, and cost have not been modelled, and a techno-economic assessment of MWCNT-based polishing trains remains an open task. We therefore moderate the scope of the practical claims: the present results indicate that, from a purely intra-particle mass-transport perspective, MWCNTs can be expected to operate in a kinetically controlled regime, but this is only one of several conditions necessary for a successful industrial deployment.

8. Conclusions

The phenomenological model parameterized with experimental equilibrium data, complemented by a sensitivity analysis and a critical discussion of model assumptions, supports the following conclusions, summarized graphically in Figure 3:

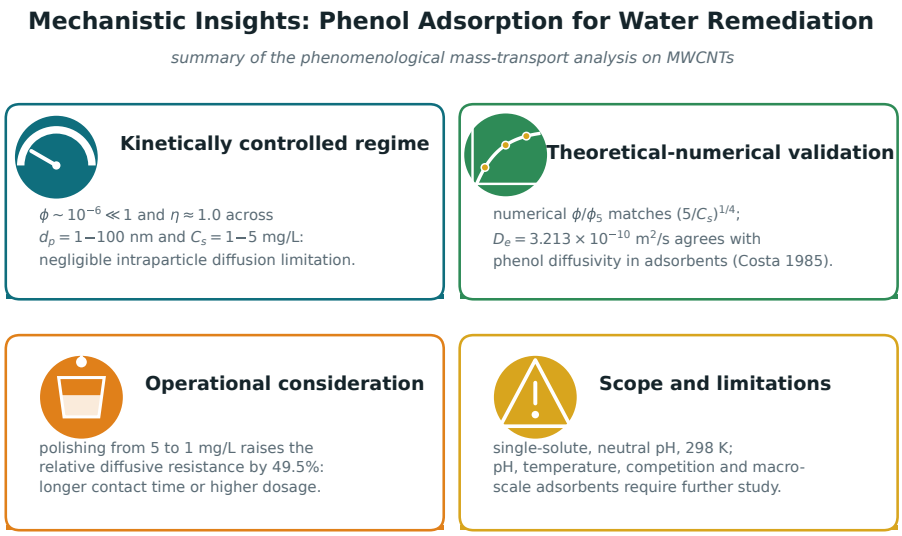

Figure 3. Graphical summary of the mechanistic insights into phenol adsorption for water remediation, highlighting the kinetically controlled regime, the theoretical–numerical validation, and the operational considerations. The literature value of the intraparticle diffusivity of phenol used for comparison is that of Costa and Rodrigues [15].

1. **Physical Adsorption:** A modified Fick's Second Law captures the coupling between intraparticle diffusion and rapid Langmuir-type site filling, leading to apparent diffusivities orders of magnitude lower than D_e. The Langmuir framework is used here as a phenomenological device, and its limitations on a heterogeneous MWCNT surface are discussed explicitly.
2. **0.5-Order Kinetics:** At neutral pH and 298 K, the Thiele modulus ($\phi \ll 1$) indicates a kinetically controlled regime with $\eta \approx 1.0$. The 0.5-order ansatz is presented as an empirical, representative simplification, and its conclusions are shown to be robust against the choice of PFO or PSO kinetics.
3. **Parametric and Sensitivity Analyses:** The linear dependence $\phi \propto R_p$ holds across the 1–100 nm range, and the scaling $\phi \propto C_s^{-0.25}$ is reproduced numerically. A one-at-a-time sensitivity analysis on D_e, κ, and k_{obs} confirms that the kinetic regime persists under the parameter perturbations tested.
4. **Theoretical Implications and Limits:** Within its domain of validity, the model indicates that intra-particle diffusional resistance is several orders of magnitude smaller than for macroscopic granular adsorbents. This is a theoretical architectural advantage. Translating it into industrial benefits will require experimental validation in real effluents, including pH variability, competitive adsorption, ionic-strength effects, and reactor- and process-level evaluations of cost, regeneration, and fouling. These remain priorities for future work.

Author Contributions: Conceptualization, T.F.d.O.; methodology, T.F.d.O.; software, T.F.d.O.; validation, T.F.d.O.; formal analysis, T.F.d.O.; writing—original draft preparation, T.F.d.O.; writing—review and editing, T.F.d.O.; supervision, S.M.P.M. All authors have read and agreed to the published version of the manuscript.

Funding: The authors gratefully acknowledge the financial support provided by the Fundação de Amparo à Pesquisa do Estado de Alagoas (FAPEAL) (Process No. E:60030.0000000584/2026).

Institutional Review Board Statement: Not applicable.

Informed Consent Statement: Not applicable.

Data Availability Statement: No new experimental data were created in this study. All input parameters were taken from the published sources cited in the text, and all numerical results reported here can be reproduced from the equations and parameter values given herein.

Conflicts of Interest: The authors declare no conflicts of interest.

Abbreviations

MWCNTs	Multi-walled Carbon Nanotubes
PFO	Pseudo-first-order kinetic model
PSO	Pseudo-second-order kinetic model
OAT	One-at-a-time (sensitivity analysis)
C	Local pore-fluid concentration of phenol [mol/m^3]
C_s	Surface (boundary) concentration of phenol [mol/m^3]
q	Adsorbed-phase concentration [mol/kg]
q_{max}	Langmuir maximum adsorption capacity [mg/kg]
K_L	Langmuir affinity constant [L/mg]
D_{AB}	Molecular diffusivity (free diffusion) [m^2/s]
D_e	Effective diffusivity (in pores) [m^2/s]
D_{app}	Apparent diffusivity (with sorption retardation) [m^2/s]
ε_p	Intraparticle porosity (–)
V_p	Specific pore volume [m^3/kg]

κ	Tortuosity factor (–)
τ	Tortuosity (–)
ρ_{true}	True graphitic density [kg/m^3]
ρ_{ap}	Apparent particle density [kg/m^3]
ρ_s	Bulk density of the packed adsorbent [kg/m^3]
R_p	Particle radius [m]
d_p	Particle diameter [nm]
k_{obs}	Apparent kinetic constant for the half-order rate law [mol$^{0.5}$ m$^{-1.5}$ s^{-1}]
ϕ	Thiele modulus (–)
η	Effectiveness factor (–)
SSA	Specific surface area [m^2/g]

References

1. Surkatti, R.; Al-Zuhair, S. Microalgae Cultivation for phenolic compounds removal. *Environ. Sci. Pollut. Res. Int.* **2018**, *25*, 33936–33956. [CrossRef] [PubMed]
2. Rai, A.; Sen, A.; Sarkar, B.; Chakrabarty, J.; Mondal, B.K.; Dutta, S. Phycoremediation of pollutants from secondary treated coke-oven wastewater using poultry litter as nutrient source: A cost-effective polishing technique. *Water Sci. Technol.* **2021**, *84*, 2406–2421. [CrossRef] [PubMed]
3. Moraes, F.D.; Figueiredo, J.S.L.; Rossi, P.A.; Venturini, F.P.; Moraes, G. Acute toxicity and sublethal effects of phenol on hematological parameters of channel catfish *Ictalurus punctatus* Pacu *Piaractus mesopotamicus*. *Ecotoxicol. Environ. Contam.* **2015**, *10*, 31–36. [CrossRef]
4. Prasun, A.; Singh, A.; Kumar, P.A.; Alam, A.; Kumar, A. Removal of Phenol from Biomedical Waste via an Adsorption Process. *Eng. Proc.* **2023**, *37*, 30. [CrossRef]
5. Vaidhyaraman, L.; Lobo, S.P.; Girish, C.R. Preparation and Characterization of Activated Carbon Using Pinecone (Conifer Cone) to Remove Phenol from Wastewater. *Eng. Proc.* **2023**, *59*, 76. [CrossRef]
6. Wang, Y.; Wang, Z.; Liu, Z.; He, X.; Zeng, Z. Mechanistic Insights into m-Cresol Adsorption on Functional Resins: Surface Chemistry and Adsorption Behavior. *Materials* **2025**, *18*, 3628. [CrossRef] [PubMed]
7. Abdel-Ghani, N.T.; El-Chaghaby, G.A.; Helal, F.S. Individual and competitive adsorption of phenol and nickel onto multiwalled carbon nanotubes. *J. Adv. Res.* **2015**, *6*, 405–415. [CrossRef] [PubMed]
8. Ceroni, L.; Benazzato, S.; Pressi, S.; Calvillo, L.; Marotta, E.; Menna, E. Enhanced Adsorption of Methylene Blue Dye on Functionalized Multi-Walled Carbon Nanotubes. *Nanomaterials* **2024**, *14*, 522. [CrossRef] [PubMed]
9. Skourti, A.; Giannoulia, S.; Daletou, M.K.; Aggelopoulos, C.A. Enhanced Dye Adsorption on Cold Plasma-oxidized Multi-Walled Carbon Nanotubes: A Comparative Study. *Nanomaterials* **2024**, *14*, 1298. [CrossRef] [PubMed]
10. Oliveira, T.F.; Meneghetti, S.M.P. Mechanistic Insights into Phenol Adsorption and Mass Transport on Multi-Walled Carbon Nanotubes. In *Proceedings of the 1st International Online Conference on Environments, 2–4 March 2026*; MDPI: Basel, Switzerland. Available online: https://sciforum.net/paper/view/28988 (accessed on 13 March 2026).
11. Plugatyr, A.; Svishchev, I.M. Molecular diffusivity of phenol in sub- and supercritical water: Application of the split-flow Taylor dispersion technique. *J. Phys. Chem. B* **2011**, *115*, 2555–2562. [CrossRef] [PubMed]
12. Epstein, N. On tortuosity and the tortuosity factor in flow and diffusion through porous media. *Chem. Eng. Sci.* **1989**, *44*, 777–779. [CrossRef]
13. van Brakel, J.; Heertjes, P.M. Analysis of diffusion in macroporous media in terms of a porosity, a tortuosity and a constrictivity factor. *Int. J. Heat Mass Transf.* **1974**, *17*, 1093–1103. [CrossRef]
14. Xie, B.; Qin, J.; Wang, S.; Li, X.; Sun, H.; Chen, W. Adsorption of Phenol on Commercial Activated Carbons: Modelling and Interpretation. *Int. J. Environ. Res. Public Health* **2020**, *17*, 789. [CrossRef] [PubMed]
15. Costa, C.; Rodrigues, A. Intraparticle diffusion of phenol in macroreticular adsorbents: Modelling and experimental study of batch and CSTR adsorbers. *Chem. Eng. Sci.* **1985**, *40*, 983–993. [CrossRef]
16. Wu, Y.; Zhang, X.; Liu, C.; Tian, L.; Zhang, Y.; Zhu, M.; Qiao, W.; Wu, J.; Yan, S.; Zhang, H.; et al. Adsorption Behaviors and Mechanism of Phenol and Catechol in Wastewater by Magnetic Graphene Oxides: A Comprehensive Study Based on Adsorption Experiments, Mathematical Models, and Molecular simulations. *ACS Omega* **2024**, *9*, 15101–15113. [CrossRef] [PubMed]

Disclaimer/Publisher's Note: The statements, opinions and data contained in all publications are solely those of the individual author(s) and contributor(s) and not of MDPI and/or the editor(s). MDPI and/or the editor(s) disclaim responsibility for any injury to people or property resulting from any ideas, methods, instructions or products referred to in the content.